SCIENTIFIC REPORTS
nature research

OPEN

Magnetic properties of six-legged spin-1 nanotube in presence of a longitudinal applied field

Received: 13 May 2019
Accepted: 13 August 2019
Published online: 26 August 2019

Zakaria ElMaddahi, Moulay Youssef El Hafidi & Mohamed El Hafidi

In this paper, we investigate the magnetic behavior of a single-walled hexagonal spin-1 Ising nanotube by using the effective field theory (EFT) with correlations and the differential operator technique (DOT). The system consists of six long legs distributed parallel to each other on a hexagonal basis. Within each chain, spin sites are regularly positioned and magnetically coupled through a $J_{//}$ exchange interaction along the chains and J⊥ between adjacent chains. Key equations of magnetization, susceptibility and critical temperatures are established, numerically resolved and carefully analyzed for some selected exchange couplings and various applied magnetic fields. In addition to the phase diagram, interesting phenomena are noted, particularly for opposite exchange interactions where magnetization plateaus and frustration are discovered.

The recent decade has seen a resurgence of interest in small-sizes magnetic objects, especially at nanoscale (nanoparticles, nanotubes, nanowires, etc.). This is due, on the one hand, to advances in atomic engineering and, on the other, to their potential applications in various fields such as magnetic drug delivery[1], bio and nanomedicine[2], nano-magnetic resonance imagery (Nano-MRI) with nanoscale resolution[3], permanent magnets[4], long-lasting memories[5] and recording media[6].

Theoretically, the magnetic properties of nanoparticles and nanotubes characterized by their quantum and surface boundary effects[7,8] have been widely investigated by the well-known methods of statistical and quantum physics including the effective field theory (EFT)[9,10], Monte Carlo (MC) simulation[11], the mean field theory (MFT)[12], Green function formalism[13] and Bethe-Peierls approximation[14]. For instance, Y. Kocakaplan *et al.* have studied the magnetic properties and hysteresis behaviors of a cylindrical transverse spin-1 Ising nanowire with a crystal field interaction in absence of magnetic field using the effective field theory combined with a probability distribution technique[15]. On the other hand, Wei Wang *et al.* have examined the compensation behaviors and magnetic properties of a cylindrical ferrimagnetic core-shell Ising nanotube by using MC simulation. The authors found that the system undergoes first- or second-order phase transitions for some physical parameters[16].

Here, we aim to study the magnetic properties of a six-legged spin-1 nanotube by applying the effective-field theory (EFT) with correlations and the differential operator technique (DOT).

Results of analytical and numerical calculations for magnetization and susceptibility are presented and carefully discussed for specific values of the exchange couplings and so the external longitudinal magnetic fields. Hence, they play a key role in nanotube magnetic properties. Also, phase diagrams of the hexagonal nanotube are investigated. Particular attention has been given to conflicting cases of exchange couplings along and between chains constituting the nanotube. Magnetic plateaus have been revealed, reflecting the frustrations that arise in such situations.

The manuscript is structured as follows: Section 2 is destined to introduce the theoretical approach of the effective field theory (EFT) with correlations, to get expressions of magnetization, internal energy, specific heat, entropy, free energy and critical boundaries in the single-wall spin-1 Ising hexagonal nanotubes. In Section 3, we present numerical results and diagrams in a ferromagnetic and antiferromagnetic state with a special focus on frustration cases. In Section 4, we formulate some concluding remarks.

Condensed Matter Physics Laboratory, Faculty of Science Ben M'sik, Hassan II University of Casablanca, B. P 7955, Av. D. El Harty, 20663, Casablanca, Morocco. Correspondence and requests for materials should be addressed to M.E. (email: mohamed.elhafidi@univh2c.ma)

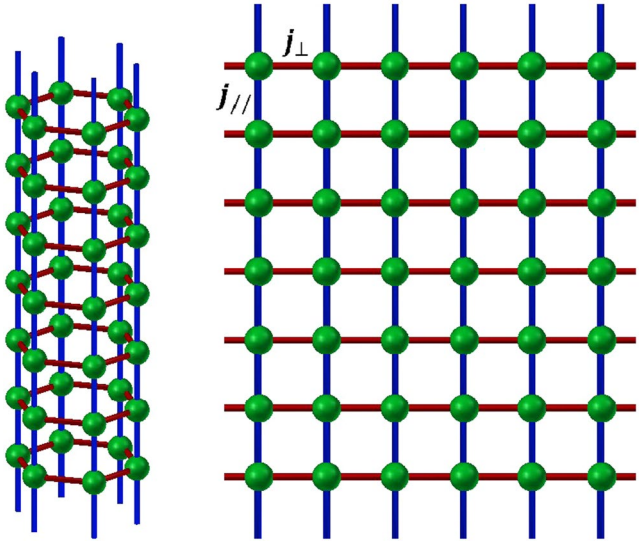

Figure 1. Schematic representation of the hexagonal spin nanotube. (**a**) The green spheres display the magnetic atoms (with spin S = 1). The blue and the red lines correspond respectively to the longitudinal exchange ($J_{//}$) and transversal exchange ($J_\perp$) coupling links. (**b**) The in-plane equivalent structure of the nanotube consisting on a six-chains grid with the periodic boundary condition in the horizontal direction $S_{i,\delta+6} \equiv S_{i,\delta}$.

Model and Theoretical Formulation

The considered model consists of a spin-1 Ising hexagonal nanotube under an external longitudinal magnetic field. The schematic stacking of the nanotube is depicted in Fig. 1. In our work, the hexagonal nanotube can be built as follows: firstly, the six chains are connected each to other forming a monolayer grid with vectors **a** and **b**, then by rolling up the monolayer along a given chiral axis $\mathbf{r} = n\mathbf{a} + m\mathbf{b}$, where **a** and **b** are the in-plane lattice vectors, n and m are two integer numbers (here n = 6 and m = 0)[17]. Thus, within the obtained hexagonal nanotube, each site is occupied by a spin-1 Ising particle and each spin (i, α) on the chain α (α = 1–6) interacts not only with its two adjacent neighbors neighbor (i ± 1, α) along the chain via the longitudinal exchange $J_{//}$ but also with its two in-plan nearest-neighbors (i, α ± 1) via the transverse component $J_\perp$.

The spin system is describing by the following Hamiltonian:

$$H = -J_\perp \sum_i^N \sum_{\delta=1}^6 S_{i,\delta} S_{i,\delta+1} - J_{//} \sum_i^N \sum_{\delta=1}^6 S_{i,\delta} S_{i+1,\delta} - h \sum_i^N \sum_\delta^6 S_{i,\delta} \tag{1}$$

where the spin operator S_z can take one of the three allowed eigenvalues: {±1, 0}. The two first sums run over entirely nearest neighbors pairs on the magnetic network. The last summation corresponds to the Zeeman coupling and is over all the lattice sites. $J_{//}$ is the longitudinal exchange interaction linking two nearest-neighbor magnetic atoms along the chains and the $J_\perp$ is the transverse exchange interaction acting among adjacent chains. $J_r > 0$ (r = //, ⊥) (respectively < 0) for ferromagnetic, FM (respectively antiferromagnetic, AFM). h is the applied longitudinal magnetic field.

In order to apply the EFT with correlations and the DOT for the considered spin-1 system, we reformulate the spin Hamiltonian in the simplest form:

$$H = -\sum_i^N \sum_\delta^6 S_{i,\delta} H_{i\delta} \tag{2}$$

where

$$H_{i\delta} = h + J_\perp \sum_{\delta' \neq \delta} S_{i,\delta'} + J_{//} \sum_{i' \neq i} S_{i',\delta} \tag{3}$$

Thus, the configurational average of spin $\langle S_{i,j} \rangle$ at the thermodynamic equilibrium is expressed within the framework of the EFT with correlations by[18]:

$$\langle S_{i,\delta} \rangle = \frac{1}{Z} Tr \left(\frac{Tr_i (S_{i,\delta} e^{-\beta H_{i\delta}})}{Tr_i (e^{-\beta H_{i\delta}})} \right) \tag{4}$$

For $S_{i\delta} = \{-1; 0; 1\}$

$$\left\langle f_{i,\delta} S_{i,\delta} \right\rangle = \left\langle f_i \frac{2\ sh(\beta E_{i\delta} + h)}{2\ ch(\beta E_{i\delta} + h) + 1} \right\rangle \tag{5}$$

$$\langle (S_{i,\delta})^2 \rangle = \left\langle \frac{2\ ch(\beta E_{i\delta} + h)}{2\ ch(\beta E_{i\delta} + h) + 1} \right\rangle \tag{6}$$

where $E_{i\delta}$ are the corresponding eigenvalues of $H_{i\delta}$.

Now, let us introduce the differential operator technique as follows

$$\left\langle f_{i,\delta} S_{i,\delta} \right\rangle = \left\langle f_{i,\delta} e^{\nabla E_{i,\delta}} \right\rangle F(x + h)\Big|_{x=0} \tag{7}$$

where $f_{i,\delta}$ designs any function of spin variables except $S_{i,\delta}$

and

$$\langle (S_{i,\delta})^2 \rangle = \langle e^{\nabla E_{i,\delta}} \rangle G(x + h)\big|_{x=0} \tag{8}$$

where $\nabla = \frac{\partial}{\partial x}$ is a differential operator. The functions $F(x+h)$ and $G(x+h)$ are defined by

$$\langle F(x + h) \rangle = \left\langle \frac{2\ sh(\beta E_{i,\delta} + h)}{2\ ch(\beta E_{i,\delta} + h) + 1} \right\rangle \tag{9}$$

$$\langle G(x + h) \rangle = \left\langle \frac{2\ ch(\beta\ E_{i\delta} + h)}{2\ ch(\beta E_{i\delta} + h) + 1} \right\rangle \tag{10}$$

By using the identity

$$e^{\alpha S_{i,\delta}} = (S_{i,\delta})^2 \mathrm{ch}(\alpha) + S_{i,\delta}\ sh(\alpha) + 1 - (S_{i,\delta})^2 \tag{11}$$

the expression value $\left\langle f_{i,\delta} e^{\nabla E_{i,\delta}} \right\rangle$ reduces to

$$\begin{aligned} \left\langle f_{i,\delta} e^{\nabla E_{i\delta}} \right\rangle \ = \ & \langle f_{i,\delta} \prod_{\delta'} [(S_{i,\delta'})^2 \mathrm{ch}(\nabla J_\perp) + S_{i,\delta'} sh(\nabla J_\perp) + 1 - (S_{i,\delta'})^2] \\ & \prod_{i'} [(S_{i',\delta})^2 \mathrm{ch}(\nabla J_{//}) + S_{i',\delta} sh(\nabla J_{//}) + 1 - (S_{i',\delta})^2] \rangle \end{aligned} \tag{12}$$

From which $\langle S_{i,\delta} \rangle$ and $\langle (S_{i,\delta})^2 \rangle$ are given by (by putting $f_{i,\delta} = 1$)

$$\begin{aligned} \langle S_{i,\delta} \rangle \ = \ & \langle \prod_{\delta'} [(S_{i,\delta'})^2 \mathrm{ch}(\nabla J_\perp) + S_{i,\delta'} sh(\nabla J_\perp) + 1 - (S_{i,\delta'})^2] \\ & \prod_{i'} [(S_{i',\delta})^2 \mathrm{ch}(\nabla J_{//}) + S_{i',\delta}\ sh(\nabla J_{//}) + 1 - (S_{i',\delta})^2] \rangle F(x + \beta h)\big|_{x=0} \end{aligned} \tag{13}$$

and

$$\begin{aligned} \langle (S_{i,\delta})^2 \rangle = \ & \langle \prod_{\delta'} [(S_{i,\delta'})^2 \mathrm{ch}(\nabla J_\perp) + S_{i,\delta'} sh(\nabla J_\perp) + 1 - (S_{i,\delta'})^2] \\ & \prod_{i'} [(S_{i',\delta})^2 \mathrm{ch}(\nabla J_{//}) + S_{i',\delta}\ sh(\nabla J_{//}) + 1 - (S_{i',\delta})^2] \rangle G(x + \beta h)\big|_{x=0} \end{aligned} \tag{14}$$

At this stage, one may evaluate the magnetization $m = <S_{i,\delta}>$ for the spin-1 nanotube, by applying delicately the effective field theory (EFT) with correlations and the differential operator technique (DOT):

$$\begin{aligned} m \ = \ & \langle \prod_{\delta'} [(S_{i,\delta'})^2 \mathrm{ch}(\nabla J_\perp) + S_{i,\delta'}\ sh(\nabla J_\perp) + 1 - (S_{i,\delta'})^2] \\ & \prod_{i'} [(S_{i',\delta})^2 \mathrm{ch}(\nabla J_{//}) + S_{i',\delta}\ sh(\nabla J_{//}) + 1 - (S_{i',\delta})^2] \rangle F(x + \beta h)\big|_{x=0} \end{aligned} \tag{15}$$

where $\beta = \frac{1}{K_B T}$, k_B being the Boltzmann constant and T the absolute temperature, $\frac{\partial}{\partial x}$ the one-dimensional differential operator which is defined by its action $e^{\gamma \frac{\partial}{\partial x}} f(x) = f(x + \gamma)$.

After long calculations, the quadrupolar moment $q = \langle (S_{i,\delta})^2 \rangle$ measuring the mutual spins correlations within the nanotube can be expressed by the following equation:

$$\begin{aligned} q \;=\; & \langle \prod_{\delta'} [(S_{i,\delta'})^2 \mathrm{ch}(\nabla J_\perp) + S_{i,\delta'}\, \mathrm{sh}(\nabla J_\perp) + 1 - (S_{i,\delta'})^2] \\ & \prod_{i'} [(S_{i',\delta})^2 \mathrm{ch}(\nabla \mathrm{J}_{//}) + S_{i',\delta}\, \mathrm{sh}(\nabla \mathrm{J}_{//}) + 1 - (S_{i',\delta})^2] \rangle G(\mathrm{x} + \beta \mathrm{h})|_{\mathrm{x}=0} \end{aligned} \tag{16}$$

by the use of the decoupling approximation[19]:

$$\left\langle S_j^z (S_k^z)^2 \;\ldots\; \ldots \;\ldots\; S_l^z \right\rangle = \left\langle S_j^z \right\rangle \langle (S_k^z)^2 \rangle \;\ldots\; \ldots \;\ldots \langle S_l^z \rangle \tag{17}$$

Thereafter, by limiting our calculations to the nearest neighbors of a given spin, the magnetization and the quadrupolar moment per site become respectively

$$\begin{aligned} \mathrm{m} \;=\; & \prod_{\delta'=1}^{2} [\mathrm{q}\ \mathrm{ch}(\nabla J_\perp) + \mathrm{m}\ \mathrm{sh}(\nabla J_\perp) + 1 - \mathrm{q}] \\ & \prod_{i'=1}^{2} [\mathrm{q}\ \mathrm{ch}(\nabla \mathrm{J}_{//}) + \mathrm{m}\ \mathrm{sh}(\nabla \mathrm{J}_{//}) + 1 - \mathrm{q}] \mathrm{F}(\mathrm{x} + \beta h)|_{\mathrm{x}=0} \end{aligned} \tag{18}$$

$$\begin{aligned} q \;=\; & \prod_{\delta'=1}^{2} [\mathrm{q}\ \mathrm{ch}(\nabla J_\perp) + \mathrm{m}\ \mathrm{sh}(\nabla J_\perp) + 1 - \mathrm{q}] \\ & \prod_{i'=1}^{2} [\mathrm{q}\ \mathrm{ch}(\nabla \mathrm{J}_{//}) + \mathrm{m}\ \mathrm{sh}(\nabla \mathrm{J}_{//}) + 1 - \mathrm{q}] G(x + \beta h)|_{x=0} \end{aligned} \tag{19}$$

Expanding the right hand side of eqs (18) and (19) and after long analytical calculations, these two keys variables can be written as

$$m = A_0 + A_1 m + A_2 m^2 + A_3 m^3 + A_4 m^4 \tag{20}$$

and

$$q = B_0 + B_1 m + B_2 m^2 + B_3 m^3 + B_4 m^4 \tag{21}$$

where A_n and $B_{n'}$ (n, n′ = 0−4) are coefficients depending on T, h, q, $J_{//}$ and $J_\perp$ (their explicit expressions are given in Annex 1).

By differentiating magnetizations with respect to h, the initial susceptibility χ can be determined from the following equation:

$$\chi(T) = \left. \frac{\partial m(T,\, h)}{\partial h} \right|_{h=0} \tag{22}$$

Note that this technique allows, in despite of its hardness, to determine other other physical variables such as internal energy, magnetic entropy, specific heat, etc. Nevertheless, here, we restrict ourselves to the magnetization and the initial susceptibility. Numerical findings will be presented and discussed in the next section.

Let us to remember that the approach of EFT combined with the DOT is evidently accurate than the mean field approximation, nevertheless its generalization to Heisenberg-type systems, where spin interacts with its neighbors in the three directions, remains delicate and difficult to put into equation[18,19].

Numerical Results and Discussions

In this section, we report our analytical and numerical investigation of the magnetization, the quadrupolar moment and the magnetic susceptibility behaviors of the system. This study will allow us to characterize the order nature of transitions as well as the main interactions roles in the spin nanotube. This makes these new materials even more promising for technological applications than previously thought.

Spontaneous magnetization. Figure 2 illustrates the thermal variation of the spontaneous magnetization obtained by solving numerically self-consistent the coupled eqs 7 and 8 for a selected set of positive transverse ($J_\perp = 3$ K) and longitudinal exchange constants ($J_{//}$ from 1 up to 5), in the absence of the external magnetic field (h = 0). Note that h is given here in energy units.

Actually, our finding is very useful in the understanding of the ferromagnetic behavior: the spontaneous magnetizations start from the same point (m = 1) and they decrease to zero at the critical temperature T_c where the system displays a Ferro-Paramagnetic (FM-PM) phase transition.

Based on the graph analysis, we can conclude that the magnetization exhibits a faster decrease from the saturation value with the decreasing of exchange interactions values. However, the value of the critical temperature T_c increases while increasing exchange interactions ($J_\perp$ and $J_{//}$), both or one of them.

Figure 3 depicts the quadrupole moment as a function of temperature, for different values of longitudinal and transverse exchange parameters. We can see that the quadrupole moments starts from 1 and decrease with the increase of temperature and an inflection point at T_c.

We note, from this figure, that typical ferromagnetic magnetization curves are obtained and that the critical temperature increases while increasing the longitudinal and/or the transversal exchange coupling.

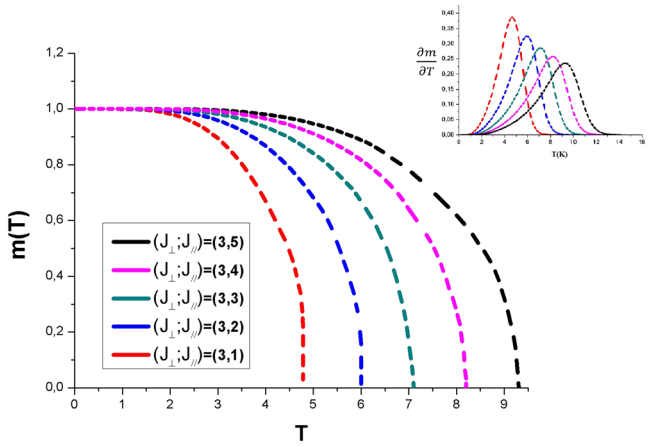

Figure 2. The spontaneous magnetization in Bohr magneton units as a function of the temperature for a selected value of $J_\perp = 3$ K and different values of $J_{//}$ from 1 up to 5 K without any external field. The inset displays details of $\left|\frac{\partial m}{\partial T}\right|$ curves.

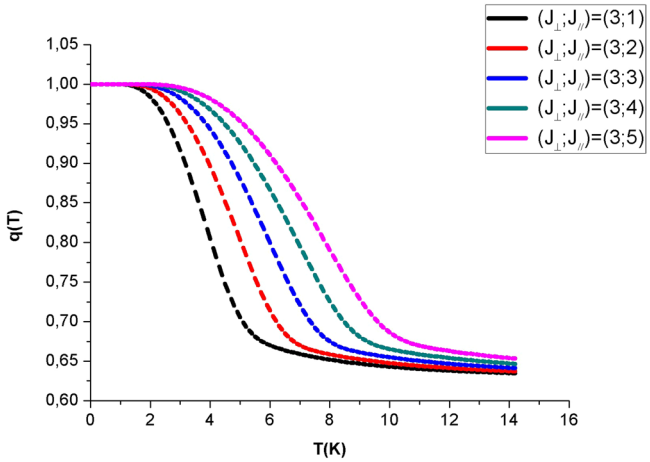

Figure 3. Temperature dependence of the quadrupole moment of the hexagonal nanotube for a selected value of the perpendicular exchange coupling $J_\perp = 3$ K and different values of $J_{//}$ from 1 up to 5 K.

Magnetic susceptibility. Magnetic susceptibility is, in general, among tools allowing the detection and the separation between different magnetic phases thanks to the characterization of the "critical temperatures" and to the quantitative ratio between phases. Figure 4 shows the plot of magnetic susceptibility against temperature for a given value of transverse exchange constant ($J_\perp = 3$ K) and various values of longitudinal exchange interaction ($J_{//}$ from 1 up to 5 K) without any applied field ($h = 0$). We notice that susceptibility increases, at first with the temperature up to a broad peak at the critical temperature for FM to PM transition and then decreases from its maximum, to weaker values with increasing temperature. This susceptibility peak is shifted to higher values when $J_{//}$ is turned on. This is quite normal since the two exchange constants are positive corresponding to the ferromagnetism, the critical temperature increases with the increase of the exchange constant. Note that the susceptibility peak matches well with the absolute order-parameter derivative $|\partial M/\partial T|$ obtained from spontaneous magnetization curves (see Fig. 2) elucidating the evidence of a second-phase order transition.

To sum up, we have drawn up in Fig. 5 a three-dimensional graph of the phase diagram for the ferromagnetic exchange case. We remark that the critical temperature is increasing monotonously with both $J_\perp$ and $J_{//}$. It is advisable to examine some standard situations, especially the case $J_\perp = J_{//} = J = 3$ K corresponding to an isotropic Ising system. We note that the value of the critical temperature found ($T_c \simeq 7.6$ K) in this case is rather close to the T_c corresponding to a 2D Ising system ($k_B T_c/J = \frac{2}{\ln(2+\sqrt{2})}$ giving $T_c \simeq 6.81$ K) than to the T_c value established by Monte Carlo simulation for a 3D Ising system where $k_B T_c/J \simeq 4.5$ giving $T_c \simeq 13.5$ K[20], whereas the critical temperature predicted by the mean field theory (MFT) is $k_B T_c = z\,J(S+1)/3S \simeq 4$ K[21].

In the next section, we will look at the situation where the exchange constants are opposite in order to highlight the frustration.

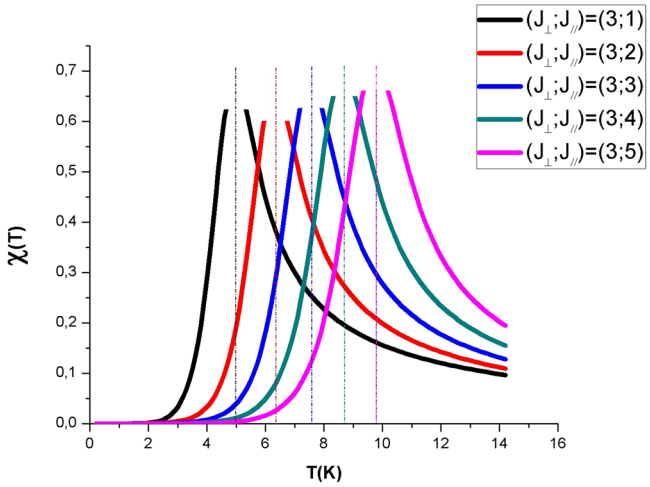

Figure 4. Magnetic susceptibility χ as a function of temperature T for the hexagonal nanotube with the fixed values of $J_{\perp} = 3$ K, $J_{//}$ from 1 up to 5 K and $h = 0$. Vertical dashed lines indicate the location of the critical temperature.

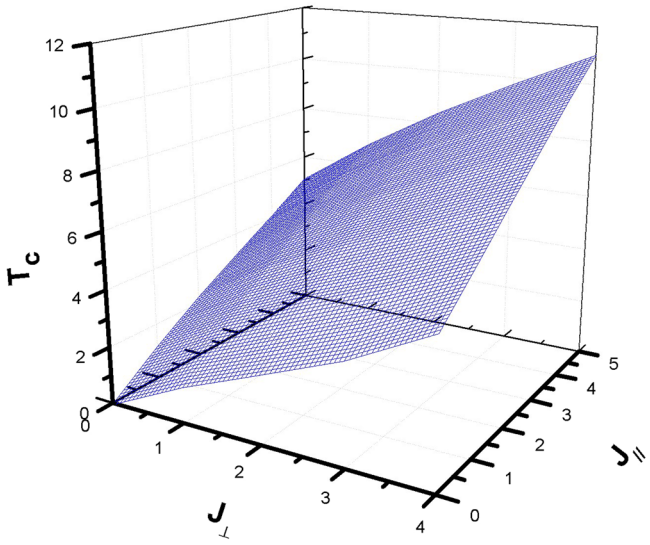

Figure 5. Three-dimensional plot of the phase diagram T_c vs ($J_{\perp}$, $J_{//}$) of the hexagonal spin-1 nanotube for the ferromagnetic case.

Magnetization plateaus: frustration signature. It should be interesting to mention that the spin-1 hexagonal nanotube may display a rather diverse magnetization process including either one, two or three intermediate magnetization plateaus when the exchange couplings are conflicting ($J_{\perp} > 0$, $J_{//} < 0$ or $J_{\perp} < 0$, $J_{//} > 0$) giving rise to frustration. It is well known that frustration is caused by the competition of ferromagnetic and antiferromagnetic couplings, or linked to the spin lattice geometry such as in triangular antiferromagnetic structures for a review see[22]. When the frustration parameter is sufficiently small, $\varepsilon = -J_{\perp}/J_{//} \leq 1$, one may observe just one intermediate plateau at a fraction of the saturation magnetization related to a ferrimagnetic phase due mainly to uncompensated ratios of $m_s = +1$, 0 and -1 spin states for $S = 1$ (see Fig. 6). When the frustration parameter is increased (for example $J_{\perp} = -6$, $J_{//} = 4$; $\varepsilon = 6/4 = 1.5$), a more spectacular magnetization curve with three different intermediate plateaus at 0.15, 0.45 and 0.5 of the saturation magnetization can be detected for moderate values of ε (see Fig. 6).

Conjointly to the magnetization plateaus observed at low temperature, sudden jumps occur at critical fields where the Zeeman contribution in the Hamiltonian (1) overcomes the frustrated exchange couplings and succeeds in tilting another proportion of spins towards their high states. This assumes the existence of energy barriers between populated levels and a residual entropy due to frustration causing quantum fluctuations. Within a plateau, the spins are confined in a highly degenerate energy band and as the field increases, the degeneracy of these levels attains its minimum degree at the saturation magnetization. At higher temperatures, the magnetization

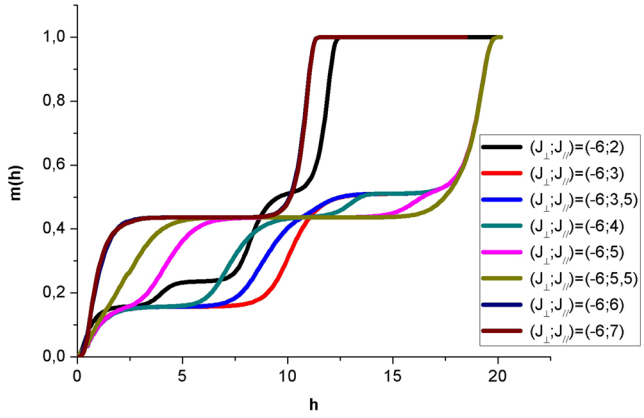

Figure 6. Low temperature (T = 0.40 K) isotherms of magnetization per site m of the hexagonal spin-1 nanotube for $J_{\perp} = -6$ K and $J_{//}$ from 2 to 7 K (ε from 3 to 0.86). *h* is given in energy units.

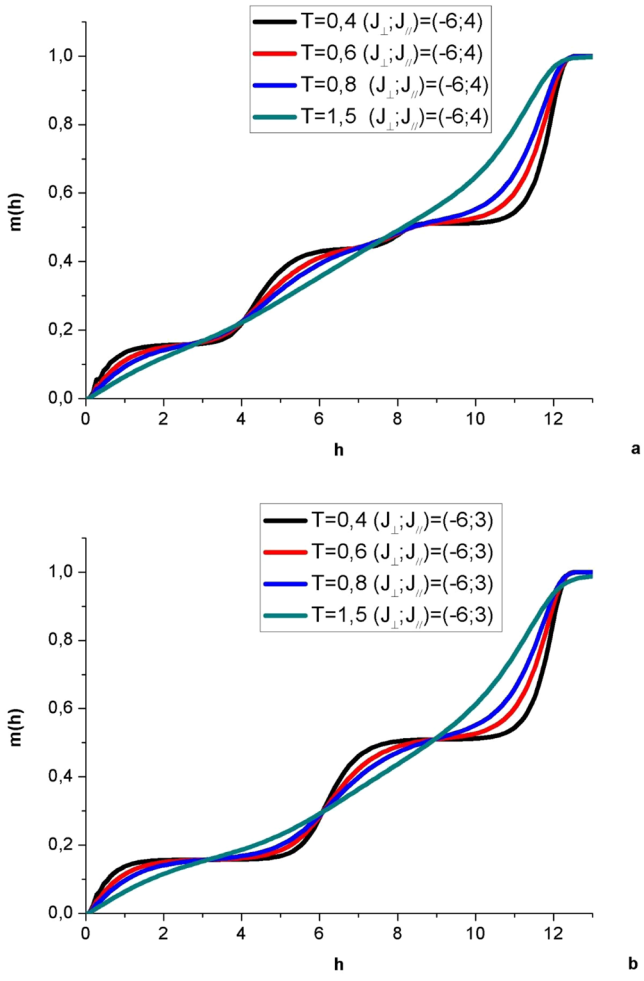

Figure 7. Magnetic field h dependence of magnetization m for the hexagonal nanotube with spin S = 1, $J_{\perp} = -6$, for two anisotropy ratio values ε = 1.5 (**a**) and ε = 2 (**b**) and T from 0.4 up to 1.5 K.

jumps begin to soften and magnetization increases gradually with the applied field showing only knees at the critical fields clearly observed at very low temperature (see Fig. 7 for ε = 1 and 1.5). These jumps tend to disappear as soon as relatively high temperatures are attained.

Experimentally, such plateaus have been observed at $1/3M_s$ and $2/3M_s$ in Cs_2CuBr_4[23] and at $1/3M_s$ in $Ba_3CoSb_2O_9$[24] that are viewed as geometrically frustrated Heisenberg S = 1/2 systems, where quantum fluctuations

may stabilize a series of spin states at simple increasing fractions of the saturation magnetization giving rise to kinks, jumps or plateaus in the magnetization curves.

Concluding Remarks

We have investigated the thermodynamic and magnetic properties of a single-walled spin-1 hexagonal by using the effective-field theory (EFT) with correlations and the differential operator technique (DOT). Magnetization, initial susceptibility and critical boundaries were obtained. The low temperature states magnetization displays up to three intermediate plateaus at fractional values of the saturation magnetization for opposed inter- and intra- chains exchange couplings (ferro- vs antiferromagnetic couplings). Frustration can introduce 'accidents' in the magnetization process of this quantum system, in the form of plateaus occurring at rational values of the magnetization. At higher temperature, thermal fluctuations smoothen magnetization jumps. The special geometrical shape of the tube provides its original properties between those of the 2D and 3D systems and in the near future, this type of nanomaterials would earn a key place in various fields of applications. Finite size effects in such systems should be significant, so it would be important to consider them both analytically and by numerical simulation.

Annex 1

The A_n (n = 0–4) coefficients used in Eq. (20) are given by

$$\begin{aligned}
A_0 &= \big[1 - 2q^4 cosh(j_{//})cosh(j_\perp)^2 + 4q^4 cosh(j_{//})cosh(j_\perp) \\
&\quad - 2q^4 cosh(j_{//})^2 cosh(j_\perp) + q^4 cosh(j_{//})^2 cosh(j_\perp)^2 \\
&\quad - 4q^3 + q^4 - 2q^4 cosh(j_{//}) + q^4 cosh(j_{//})^2 + 2qcosh(j_{//}) \\
&\quad + 6q^3 cosh(j_{//}) - 2q^3 cosh(j_{//})^2 + 6q^2 - 6q^2 cosh(j_{//}) \\
&\quad + q^2 cosh(j_{//})^2 - 2q^4 cosh(j_\perp) + q^4 cosh(j_\perp)^2 + q^2 cosh(j_\perp)^2 \\
&\quad + 6q^3 cosh(j_\perp) - 2q^3 cosh(j_\perp)^2 - 6q^2 cosh(j_\perp) \\
&\quad + 2q^3 cosh(j_{//})^2 cosh(j_\perp) - 8q^3 cosh(j_{//})cosh(j_\perp) \\
&\quad + 2q^3 cosh(j_{//})cosh(j_\perp)^2 + 4q^2 cosh(j_{//})cosh(j_\perp) \\
&\quad + 2qcosh(j_\perp) - 4q]F(x + \beta h)|_{x=0}
\end{aligned}$$

$$\begin{aligned}
A_1 &= \big[2sinh(j_\perp) + 2sinh(j_{//}) - 6sinh(j_{//})q - 6sinh(j_\perp)q - 2sinh(j_\perp)q^3 cosh(j_{//})^2 \\
&\quad + 4sinh(j_\perp)q^3 cosh(j_{//}) + 2sinh(j_{//})q^3 cosh(j_{//}) - 8sinh(j_\perp)q^2 cosh(j_{//}) \\
&\quad - 4sinh(j_{//})q^2 cosh(j_{//}) + 2sinh(j_{//})qcosh(j_{//}) + 2sinh(j_\perp)q^2 cosh(j_{//})^2 \\
&\quad + 2sinh(j_\perp)qcosh(j_\perp) - 4sinh(j_\perp)q^2 cosh(j_\perp) + 2sinh(j_\perp)q^3 cosh(j_\perp) \\
&\quad + 4sinh(j_{//})qcosh(j_\perp) - 8sinh(j_{//})q^2 cosh(j_\perp) + 2sinh(j_{//})q^2 (cosh(j_\perp))^2 \\
&\quad + 4sinh(j_{//})q^3 cosh(j_\perp) - 2sinh(j_{//})q^3 (cosh(j_\perp))^2 \\
&\quad + 4sinh(j_\perp) * q^2 cosh(j_{//})cosh(j_\perp) - 4sinh(j_\perp)q^3 cosh(j_{//})cosh(j_\perp) \\
&\quad + 2sinh(j_\perp)q^3 \big(cosh(j_{//})\big)^2 cosh(j_\perp) + 4sinh(j_{//})q^2 cosh(j_{//})cosh(j_\perp) \\
&\quad - 4sinh(j_{//})q^3 cosh(j_{//})cosh(j_\perp) + 2sinh(j_{//})q^3 cosh(j_{//})(cosh(j_\perp))^2 \\
&\quad - 2sinh(j_\perp)q^3 - 2sinh(j_{//})q^3 + 6sinh(j_{//})q^2 + 6sinh(j_\perp)q^2 \\
&\quad + 4sinh(j2)qcosh(j_{//})\big]F(x + \beta h)_{x=0}
\end{aligned}$$

$$\begin{aligned}
A_2 &= \big[sinh(j_\perp)^2 - 2sinh(j_\perp)^2 q + 2sinh(j_\perp)^2 qcosh(j_{//}) + sinh(j_\perp)^2 q^2 \\
&\quad - 2sinh(j_\perp)^2 q^2 cosh(j_{//}) + sinh(j_\perp)^2 q^2 cosh(j_{//})^2 + 4sinh(j_{//})sinh(j_\perp) \\
&\quad - 8sinh(j_{//})sinh(j_\perp)q + 4sinh(j_{//})sinh(j_\perp)\, q\, cosh(j_\perp) \\
&\quad + 4sinh(j_{//})sinh(j_\perp)q^2 - 4sinh(j_{//})sinh(j_\perp)q^2 cosh(j_\perp) \\
&\quad + 4sinh(j_{//})sinh(j_\perp)qcosh(j_{//}) - 4sinh(j_{//})sinh(j_\perp)q^2 cosh(j_{//}) \\
&\quad + 4sinh(j_{//})sinh(j_\perp)q^2 cosh(j_{//})cosh(j_\perp) + sinh(j_{//})^2 - 2\, sinh(j_{//})^2 q \\
&\quad + 2sinh(j_{//})^2 qcosh(j_\perp) + sinh(j_{//})^2 q^2 - 2sinh(j_{//})^2 q^2 cosh(j_\perp) \\
&\quad + sinh(j_{//})^2 q^2 cosh(j_\perp)^2\big]F(x + \beta h)|_{x=0}
\end{aligned}$$

$$A_3 = \Big[2sinh(j_{//})sinh(j_\perp)^2 - 2sinh(j_{//})sinh(j_\perp)^2 q + 2sinh(j_{//})sinh(j_\perp)^2 qcosh(j_{//}) + 2sinh(j_{//})^2 sinh(j_\perp) - 2sinh(j_{//})^2 sinh(j_\perp)q + 2sinh(j_{//})^2 sinh(j_\perp)qcosh(j_\perp)\Big]F(x+\beta h)|_{x=0}$$

$$A_4 = [sinh(j_{//})^2 sinh(j_\perp)^2]F(x+\beta h)|_{x=0}$$

while the $B_{n'}$ (n′ = 0–4) coefficients displayed in equation (21) are given as follows

$$B_0 = \Big[1 - 2q^4 cosh(j_{//})cosh(j_\perp)^2 + 4q^4 cosh(j_{//})cosh(j_\perp) - 2q^4 cosh(j_{//})^2 cosh(j_\perp) + q^4 cosh(j_{//})^2 cosh(j_\perp)^2 - 4q^3 + q^4 - 2q^4 cosh(j_{//}) + q^4 cosh(j_{//})^2 + 2qcosh(j_{//}) + 6q^3 cosh(j_{//}) - 2q^3 cosh(j_{//})^2 + 6q^2 - 6q^2 cosh(j_{//}) + q^2 cosh(j_{//})^2 - 2q^4 cosh(j_\perp) + q^4 cosh(j_\perp)^2 + q^2 cosh(j_\perp)^2 + 6q^3 cosh(j_\perp) - 2q^3 cosh(j_\perp)^2 - 6q^2 cosh(j_\perp) + 2q^3 cosh(j_{//})^2 cosh(j_\perp) - 8q^3 cosh(j_{//})cosh(j_\perp) + 2q^3 cosh(j_{//})cosh(j_\perp)^2 + 4q^2 cosh(j_{//})cosh(j_\perp) + 2qcosh(j_\perp) - 4q\Big]G(x+\beta h)|_{x=0}$$

$$B_1 = \Big[2sinh(j_\perp) + 2sinh(j_{//}) - 6sinh(j_{//})q - 6sinh(j_\perp)q - 2sinh(j_\perp)q^3 cosh(j_{//})^2 + 4sinh(j_\perp)q^3 cosh(j_{//}) + 2sinh(j_{//})q^3 cosh(j_{//}) - 8sinh(j_\perp)q^2 cosh(j_{//}) - 4sinh(j_{//})q^2 cosh(j_{//}) + 2sinh(j_{//})qcosh(j_{//}) + 2sinh(j_\perp)q^2 cosh(j_{//})^2 + 2sinh(j_\perp)qcosh(j_\perp) - 4sinh(j_\perp)q^2 cosh(j_\perp) + 2sinh(j_\perp)q^3 cosh(j_\perp) + 4sinh(j_{//})qcosh(j_\perp) - 8sinh(j_{//})q^2 cosh(j_\perp) + 2sinh(j_{//})q^2(cosh(j_\perp))^2 + 4sinh(j_{//})q^3 cosh(j_\perp) - 2sinh(j_{//})q^3(cosh(j_\perp))^2 + 4sinh(j_\perp) * q^2 cosh(j_{//})cosh(j_\perp) - 4sinh(j_\perp)q^3 cosh(j_{//})cosh(j_\perp) + 2sinh(j_\perp)q^3\Big(cosh(j_{//})\Big)^2 cosh(j_\perp) + 4sinh(j_{//})q^2 cosh(j_{//})cosh(j_\perp) - 4sinh(j_{//})q^3 cosh(j_{//})cosh(j_\perp) + 2sinh(j_{//})q^3 cosh(j_{//})(cosh(j_\perp))^2 - 2sinh(j_\perp)q^3 - 2sinh(j_{//})q^3 + 6sinh(j_{//})q^2 + 6sinh(j_\perp)q^2 + 4sinh(j2)qcosh(j_{//})\Big]G(x+\beta h)|_{x=0}$$

$$B_2 = \Big[sinh(j_\perp)^2 - 2sinh(j_\perp)^2 q + 2sinh(j_\perp)^2 qcosh(j_{//}) + sinh(j_\perp)^2 q^2 - 2sinh(j_\perp)^2 q^2 cosh(j_{//}) + sinh(j_\perp)^2 q^2 cosh(j_{//})^2 + 4sinh(j_{//})sinh(j_\perp) - 8sinh(j_{//})sinh(j_\perp)q + 4sinh(j_{//})\,sinh(j_\perp)\,q\,cosh(j_\perp) + 4sinh(j_{//})sinh(j_\perp)q^2 - 4sinh(j_{//})sinh(j_\perp)q^2 cosh(j_\perp) + 4sinh(j_{//})sinh(j_\perp)qcosh(j_{//}) - 4sinh(j_{//})sinh(j_\perp)q^2 cosh(j_{//}) + 4sinh(j_{//})sinh(j_\perp)q^2 cosh(j_{//})cosh(j_\perp) + sinh(j_{//})^2 - 2\,sinh(j_{//})^2 q + 2sinh(j_{//})^2 qcosh(j_\perp) + sinh(j_{//})^2 q^2 - 2sinh(j_{//})^2 q^2 cosh(j_\perp) + sinh(j_{//})^2 q^2 cosh(j_\perp)^2\Big]G(x+\beta h)|_{x=0}$$

$$B_3 = \Big[2sinh(j_{//})sinh(j_{\perp})^2 - 2sinh(j_{//})sinh(j_{\perp})^2 q + 2sinh(j_{//})sinh(j_{\perp})^2 qcosh(j_{//}) + 2sinh(j_{//})^2 sinh(j_{\perp}) - 2sinh(j_{//})^2 sinh(j_{\perp})q + 2sinh(j_{//})^2 sinh(j_{\perp})qcosh(j_{\perp})\Big]G(x + \beta h)|_{x=0}$$

$$B_4 = [sinh(j_{//})^2 sinh(j_{\perp})^2]G(x + \beta h)|_{x=0}$$

References

1. Pondman, K. M. *et al*. Magnetic drug delivery with FePd nanowires. *Journal of Magnetism and Magnetic Materials* **380**, 299–306 (2015).
2. Roca, A. G. *et al*. Progress in the preparation of magnetic nanoparticles for applications in biomedicine. *Journal of Physics D: Applied Physics* **42**(22), 224002 (2009).
3. Rosa, L., Blackledge, J. & Boretti, A. Nano-Magnetic Resonance Imaging (Nano-MRI) Gives Personalized Medicine a New Perspective. *Biomedicines* **5**(1), 7 (*2017*).
4. Zeng, H., Li, J., Liu, J. P., Wang, Z. L. & Sun, S. Exchange-coupled nanocomposite magnets by nanoparticle self-assembly. *Nature* **420**(6914), 395 (2002).
5. Fuhrer, M. S., Kim, B. M., Dürkop, T. & Brintlinger, T. High-mobility nanotube transistor memory. *Nano letters* **2**(7), 755–759 (2002).
6. Ray, S. C. *et al*. High coercivity magnetic multi-wall carbon nanotubes for low-dimensional high-density magnetic recording media. *Diamond and Related Materials* **19**(5-6), 553–556 (2010).
7. Thanh, N. T. Magnetic Nanoparticles: From Fabrication to Clinical Applications. 1st Edition. Pub location Boca Raton. (2012).
8. Fiorani, D. Surface Effects in Magnetic Nanoparticles: Nanostructure Science and Technology. 1st Edition. Pub Springer US. Springer-Verlag US. (2005).
9. Santos, J. P. & Barreto, F. S. An effective-field theory study of trilayer Ising nanostructure: Thermodynamic and magnetic properties. *Journal of Magnetism and Magnetic Materials* **439**, 114–119 (2017).
10. Kantar, E. & Keskin, M. Thermal and magnetic properties of ternary mixed Ising nanoparticles with core–shell structure: Effective-field theory approach. *Journal of Magnetism and Magnetic Materials* **349**, 165–172 (2014).
11. Wang, W., Lv, D., Zhang, F., Bi, J. L. & Chen, J. N. Monte Carlo simulation of magnetic properties of a mixed spin-2 and spin-5/2 ferrimagnetic Ising system in a longitudinal magnetic field. *Journal of Magnetism and Magnetic Materials* **385**, 16–26 (2015).
12. Parente, W. E., Pacobahyba, J. T. M., Neto, M. A., Araújo, I. G. & Plascak, J. A. Spin-1/2 anisotropic Heisenberg antiferromagnet model with Dzyaloshinskii-Moriya interaction via mean-field approximation. *Journal of Magnetism and Magnetic Materials* **462**, 8–12 (2018).
13. Mercaldo, M. T., Rabuffo, I., De Cesare, L. & D'Auria, A. C. Reentrant behaviors in the phase diagram of spin-1 planar ferromagnets with easy-axis single-ion anisotropy via the Devlin two-time Green function framework. *Journal of Magnetism and Magnetic Materials* **439**, 333–342 (2017).
14. Belokon, V., Kapitan, V. & Dyachenko, O. The combination of the random interaction fields method and the Bethe–Peierls method for studying two-sublattice magnets. *Journal of Magnetism and Magnetic Materials* **401**, 651–655 (2016).
15. Kocakaplan, Y., Kantar, E. & Keskin, M. Hysteresis loops and compensation behavior of cylindrical transverse spin-1 Ising nanowire with the crystal field within effective-field theory based on a probability distribution technique. *The European Physical Journal B* **86**(10), 420 (2013).
16. Wang, W. *et al*. Compensation behaviors and magnetic properties in a cylindrical ferrimagnetic nanotube with core-shell structure: A Monte Carlo study. *Physica E: Low-dimensional Systems and Nanostructures* **101**, 110–124 (2018).
17. Saito, R., Fujita, M., Dresselhaus, G. & Dresselhaus, U. M. Electronic structure of chiral graphene tubules. *Applied physics letters* **60**(18), 2204–2206 (1992).
18. Kaneyoshi, T. Differential operator technique in the Ising spin systems. *Acta Physica Polonica Series A* **83**(6), 703–7038, https://doi.org/10.12693/APhysPolA.83.703 (1993).
19. Zernike, F. The propagation of order in co-operative phenomena: Part I. The AB case. *Physica* **7**(7), 565–585 (1940).
20. Ferrenberg, A. M. & Landau, D. P. Critical behavior of the three-dimensional Ising model: A high-resolution Monte Carlo study. *Physical Review B* **44**(10), 5081 (1991).
21. Fox, P. F. & Guttmann, A. J. Low temperature critical behaviour of the Ising model with spin S > 1/2. *Journal of Physics C: Solid State Physics* **6**(5), 913 (1973).
22. Chalker, J. T., Lacroix, C., Mendels, P. & Mila, F. *Introduction to Frustrated Magnetism: Materials, Experiments, Theory*. Eds (Springer-Verlag, Berlin, 2011).
23. Fortune, N. A. *et al*. Cascade of magnetic-field-induced quantum phase transitions in a spin-1 2 triangular-lattice antiferromagnet. *Physical review letters* **102**(25), 257201 (2009).
24. Susuki, T. *et al*. Magnetization process and collective excitations in the S = 1/2 triangular-lattice Heisenberg antiferromagnet Ba 3 CoSb 2 O 9. *Physical review letters* **110**(26), 267201 (2013).

Author Contributions

Z. Elmaddahi and M.Y. El Hafidi performed analytical and numerical calculations and contributed to analyzing the numerical results. M. El Hafidi proposed the project, wrote the initial version of the manuscript and contributed to analyze data. All authors commented, critically reviewed and approved the final manuscript.

Additional Information

Competing Interests: The authors declare no competing interests.

Publisher's note: Springer Nature remains neutral with regard to jurisdictional claims in published maps and institutional affiliations.